

Article

Insight into Significance of Bioconvection on MHD Tangent Hyperbolic Nanofluid Flow of Irregular Thickness across a Slender Elastic Surface

Muhammad Zeeshan Ashraf ^{1,†}, Saif Ur Rehman ², Saadia Farid ¹, Ahmed Kadhim Hussein ³, Bagh Ali ^{4,5}, Nehad Ali Shah ^{6,†} and Wajaree Weera ^{7,*}

¹ Department of Mathematics, University of Engineering and Technology, Lahore 54890, Pakistan; zeeshan.ashraf88005@gmail.com (M.Z.A.); sadia@uet.edu.pk (S.F.)

² Department of Mathematics, University of Management and Technology, Lahore 54770, Pakistan; saifurrehman8684@gmail.com

³ Mechanical Engineering Department, College of Engineering, University of Babylon, Hilla 00964, Iraq; ahmedkadhim7474@gmail.com

⁴ Department of Applied Mathematics, Northwestern Polytechnical University, Xi'an 710072, China; baghalisewag@gmail.com

⁵ Faculty of Computer Science and Information Technology, Superior University, Lahore 54000, Pakistan

⁶ Department of Mechanical Engineering, Sejong University, Seoul 05006, Korea; nehadali199@yahoo.com

⁷ Department of Mathematics, Faculty of Science, Khon Kaen University, Khon Kaen 40002, Thailand

* Correspondence: wajawe@kku.ac.th

† These authors contributed equally to this work and are co-first authors.

Abstract: This numerical investigation effectively establishes a unique computing exploration for steady magnetohydrodynamic convective streams of tangent hyperbolic nanofluid traveling across a nonlinearly elongating elastic surface with a variable thickness. In addition, the importance of an externally imposed magnetic field of tangent hyperbolic nanofluid is comprehensively analyzed by considering the substantial impact of thermal conductivity and thermal radiation consequences. The governing PDEs (partial differential equations) are transmuted into a nonlinear differential structure of coupled ODEs (ordinary differential equations) using a series of variable similarity transformations. Furthermore, these generated ODEs (ordinary differential equations) are numerically set using a novel revolutionary Runge-Kutta algorithm with a shooting approach constructed in a MATLAB script. In this regard, extensive comparison studies are carried out to validate the acquired numerical results. The interactions between the associated profiles and the relevant parameters are rationally explored and shown using graphs and tabular forms. The velocity distribution declined with improving Weissenberg number We and power-law index m , while the reverse performance can be observed for temperature. As enhancement in Brownian motion, Thermophoretic and radiation parameters significantly rise in temperature distribution. The use of many different technological and industrial systems, including nano-bioconvective systems, nano-droplet evaporation, nano-ink jet printing, and microbial fuel cells, would benefit this research study.

Keywords: tangent hyperbolic nanofluid; bioconvection; magnetohydrodynamic; slender elastic sheet

MSC: 76D05; 35Q30



Citation: Ashraf, M.Z.; Rehman, S.U.; Farid, S.; Hussein, A.K.; Ali, B.; Shah, N.A.; Weera, W. Insight into Significance of Bioconvection on MHD Tangent Hyperbolic Nanofluid Flow of Irregular Thickness across a Slender Elastic Surface. *Mathematics* **2022**, *10*, 2592. <https://doi.org/10.3390/math10152592>

Academic Editor: Antonio Lamura

Received: 21 June 2022

Accepted: 21 July 2022

Published: 25 July 2022

Publisher's Note: MDPI stays neutral with regard to jurisdictional claims in published maps and institutional affiliations.



Copyright: © 2022 by the authors. Licensee MDPI, Basel, Switzerland. This article is an open access article distributed under the terms and conditions of the Creative Commons Attribution (CC BY) license (<https://creativecommons.org/licenses/by/4.0/>).

1. Introduction

Nanofluids are nanoparticles with diameters ranging from 1–100 nm (such as carbon nanotube CNT, iron oxide, silver, copper, titanium oxide, alumina oxide, and oxide) dispersed in base fluids (such as industry oil, alcohol, carboxymethyl cellulose CMC and water) [1,2]. Researchers have shown a great deal of interest in nanofluid throughout

the years, which has resulted in an avalanche of discoveries and inquiries into its unique features and potential applications. Recent technological advancement demonstrates that nanofluids have the potential to be used in the manufacture of automobiles, aero-planes, microreactors, and other things. Choi et al. [3] presented the concept of nanofluids for the first time in 1995, with the purpose of boosting heat transport rates. Waqas et al. [4] investigated the aspects of stratified mixed radiative-convective nanofluid stream incorporating motile microbes that are affected by the activation energy and magnetic field. This work addressed the impacts of the thermosolutal convection of solid particles. Aly et al. [5] deliberated the influence of a magnetic field on nanofluid propagating inside a finned cavity. Danial et al. [6] explored the impacts of the nanofluid on both the rate of concentration transportation (Sherwood number) and the rate of heat transference (Nusselt number). Across an infinite horizontal surface, Jamshed et al. [7] presented the formation of entropy in the magnetohydrodynamic stream of Maxwell nanofluid numerically. In this model, external factors such as viscous dissipation are also taken. The effect of employing passive approaches on the thermal transport and pressure drop efficiency of nanofluid heat transfer devices has been elaborated by Awais et al. [8]. The molecular dynamics model is used to depict the atomic behavior of nanofluid in a microchannel by Shang et al. [9] numerically. In this work, the atomic mobility of H_2O/CuO nanofluid particles increases as microchannel walls thicken and nanoparticle aggregation occurs. Dawar et al. [10] explored the impacts of a binary chemical reaction and Arrhenius activation energy on nanofluid thin film in the existence of solar radiation across a spinning disk. Sabu et al. [11] investigated the flow of alumina-water nanofluid by considering varied nanoparticles form across a rotating disk.

Bioconvection is observed when microbes migrate randomly in a single-celled and even sometimes colony-like configuration. It causes a significant rise in the buoyancy of fluid due to upstream gyrotactic microbes. Thus, it has attracted researchers' attention due to its widespread use in engineering, biological and chemical fields such as biofuels, enzymes, biotechnological applications, cancer treatment, manufacturing and production, industrial level, and others. Imran et al. [12] deliberated the physical aspects of bioconvection in a nanofluid flow comprising motile microorganisms via a parabolize horizontal surface. Waqas et al. [13] numerically studied the 2-D bioconvection tangent hyperbolic nanofluid stream along a Riga plate having gyrotactic microorganisms. Zhang et al. [14] discussed the rheological behavior of bioconvective nano liquid flow immerse in Darcy-Forchheimer medium. This article covers mixed convection, motile microorganisms, solutal boundary conditions, and activation energy. Across an exponentially stretched surface, the impacts of heat radiation and bioconvection of microbes discussed by Asjad et al. [15]. Narsimulu et al. [16] consulted the numerical technique on MHD Carreau fluid stream for increased mass transportation of bioconvection over a non-linear extending surface. This model discussed and determined the effect of controlling parameters on concentration, temperature, motile microbes and velocity, heat transmission, and skin friction. Habib et al. [17] investigated the bioconvection and radiation effects on the time-dependent magnetohydrodynamics nanofluids across an expanding sheet. Very recently, many researchers work on bioconvection using various types of geometries [18–21].

Because of its many uses in the food, polymer sectors, and paint, the viscous non-Newtonian fluid is becoming useful to researchers. The quest for a solution to the motion of a non-Newtonian fluid regulating the physical model piques intellectual curiosity. Non-Newtonian fluids include food, some oils, polymer melts, drilling muds, coatings, etc. Calculating the shearing stress and rate of strain numerically for any non-Newtonian fluid is challenging. That is why, in recent years, the tangent hyperbolic fluid model has gained popularity among scholars. Hassan et al. [22] deliberated the transportation of heat energy with structure of non-Newtonian mass under two different flow conditions. In this model, the speed and thermal profiles, including the Nusselt number and the skin friction coefficient, are glanced at under two different flow rates. In a chaotic channel, Selimefendigil et al. [23] explored the capability characteristics of the thermoelectric

system with non-newtonian fluid utilizing the FEM (finite element method) numerically. Li et al. [24] investigated the mixed convective non-newtonian fluid numerically over cylindrical shape battery with various outlet positions. Khader et al. [25] studied a 2D MHD (Magnetohydrodynamic) Casson fluid model across an extending sheet in the presence of a mixed convection heat transference method. The coupled impacts of heat radiation and magnetic fields are taken into account in this scenario. Pandey et al. [26] investigated shear-thinning non-newtonian fluids' thermal and flow properties within the heated square cavity by doing experiments and using numerical simulations. By applying the fixed point technique, Boukrouche et al. [27] discussed the unsteady non-newtonian fluid by considering shear thickening fluids with friction type boundary conditions. Colak et al. [28] deliberated the bioconvective flow of Maxwell nanofluid and the temperature-dependent viscosity with Arrhenius activation energy on it by utilizing the artificial intelligence technique. Khashi'ie et al. [29] presented the upshot of viscous dissipation and MHD (Magnetohydrodynamic) on heat transportation of non-Newtonian fluid across a shrinking surface. This model shows the similarity solutions for thermal distribution and the skin friction coefficient and temperature and velocity profiles in this model.

In the production of petroleum and the metallurgical process, magnetohydrodynamic (MHD) flow is critical. It's worth mentioning that the pace at which these processes cool influences the final output. This field of magnetism is used to distinguish metallic elements from nonmetallic components in molten metals. MHD (Magnetohydrodynamic) has applications in medicine, astronomy, advanced aircraft design, and successfully dealing with thermal transportation rates in cylinders, various machines, turbulent pumps, and energy producers. Bhatti et al. [30] elaborated on MHD Williamson nanofluid immersed in porous media via circular rotational plates in the existence of swimming gyrotactic microbes. In this work, fluid flow through circular plates is vital because they contain numerous physical mechanisms. Farhany et al. [31] deliberated the effect of MHD (Magnetohydrodynamic) on natural convection with a nano liquid porous media, including an inclined magnetic field utilizing finite element technique numerically. Bejawada et al. [32] probed the impact of chemical reactions, heat radiation, and sources on MHD Casson fluid stream across nonlinear extending surface via Forchheimer permeable media. Hossain et al. [33] explored the unsteady mixed convective time-dependent thermophysical properties of CNT (carbon nanotube) nanofluid through MHD and heat flux. Kouz et al. [34] explored a stable 2-D MHD fluid stream caused by the stretching sheet of porous media by taking into consideration heat and mass transportation. By utilizing perturbation methodology, Nazeer et al. [35] elaborated on the MHD (Magnetohydrodynamic) electro-osmotic stream of non-Newtonian MHD flow and its influence on the third-grade fluid within a micro-channel. Ramana et al. [36] analyzed the flow of MHD Oldroyd-B liquid across the stretched surface by the Cattaneo-Christov model. The thermal conductivity and heat generation effects are taken into account in this model. The stream of electrically conducting MHD nano liquid, Famakinwa et al. [37] explored numerically across a convectively thermal surface, including gyrotactic microbes. In the existence of a heat source, Fetecau et al. [38] investigated the hydromagnetic free convective flow comprising mass, chemical reaction, and Newtonian heating across a vertical plate.

We intend to simulate and investigate the steady magnetohydrodynamic flow of tangent hyperbolic nanofluid across a slender elastic surface of irregular thickness with heat radiation, inspired by the previous work. The modest diffusion of gyrotactic microorganisms is thought to be unaffected by nanoparticles. Nanoparticles are uniformly distributed throughout the base fluid. The Runge-Kutta technique is used to get numerical solutions for nonlinear coupled differential equations. Thermal transport is used in various industries, including business and engineering, microelectronics, electronic device cooling, transportation, and fuel cells. Nanofluids are a new energy transmission fluid with nanoscale particles floating in a base fluid. Nanofluids have a variety of applications, including electrical devices, manufacture of thermal exchangers, biomedicine, and engine cooling.

2. Mathematical Formulation

The present study for nanofluid flow arrangement may be seen in Figure 1 geometrically. A steady 2-D magnetohydrodynamic flow of a tangent hyperbolic nanofluid with temperature-dependent thermal conductivity across a slender elastic surface of irregular thickness $\epsilon(x) = 2c(x + b)^{\frac{1-n}{2}}$. The thin sheet is stretched upwards by a homogeneous gravitational field of strength g . The stretched sheet is heated in an unbalanced pattern due to the varying wall temperature T_w . The variable magnetic field is $B(x) = B_0(x + b)^{\frac{n-1}{2}}$ in y -direction. Furthermore, the temperature in the free-stream zone is kept constant at T_{inf} , implying that the nanofluid is in a quasi-rest condition. According to physical assumptions, the Tangent hyperbolic nanofluid has a poor electrical performance, with a negligible magnetic Reynolds number in its MHD convective motion. The origin O is located at layer transverse section center top edge—the x -axis horizontally down the elastic sheet’s symmetry axis as well as the y -axis perpendicular to the streamwise direction. We assume that the inclusion of nanoparticles does not affect the swimming velocity of the microorganisms floating in the fluid. The continuous model of Hillesdon and Pedley [39] is used to simulate bioconvective transport with oxytactic bacteria. The boundary layer theory’s set of equations is represented as [40–42].

$$\frac{\partial \hat{u}}{\partial x} + \frac{\partial \hat{v}}{\partial y} = 0, \tag{1}$$

$$\begin{aligned} \left(\hat{u} \frac{\partial \hat{u}}{\partial x} + \hat{v} \frac{\partial \hat{u}}{\partial y} \right) &= \nu(1 - m) \left(\frac{\partial^2 \hat{u}}{\partial y^2} \right) + \sqrt{2} \Gamma \nu m \left(\frac{\partial \hat{u}}{\partial y} \right) \left(\frac{\partial^2 \hat{u}}{\partial y^2} \right) - \frac{\sigma B^2(x)}{\rho} \\ &+ g[\beta \rho_f(1 - C_\infty)(T - T_\infty) - (\rho_p - \rho_f)(C - C_\infty) - \gamma(\rho_m - \rho_f)(n - n_\infty)], \end{aligned} \tag{2}$$

$$(\rho C_p)_f \left(\hat{u} \frac{\partial T}{\partial x} + \hat{v} \frac{\partial T}{\partial y} \right) = k_T \frac{\partial^2 T}{\partial y^2} + \left(\frac{\partial k_T}{\partial T} \right) \left(\frac{\partial T}{\partial y} \right)^2 + \tau \left[D_B \frac{\partial C}{\partial y} + \frac{D_T}{T_\infty} \left(\frac{\partial T}{\partial y} \right)^2 \right] + \frac{\partial qr}{\partial y}, \tag{3}$$

$$\hat{u} \frac{\partial C}{\partial x} + \hat{v} \frac{\partial C}{\partial y} = \frac{D_T}{T_\infty} \frac{\partial^2 T}{\partial y^2} + D_B \frac{\partial^2 C}{\partial y^2}, \tag{4}$$

$$\hat{u} \frac{\partial n}{\partial x} + \hat{v} \frac{\partial n}{\partial y} - D_n \left(\frac{\partial^2 n}{\partial y^2} \right) = \frac{dw_c}{C_w - C_\infty} \frac{\partial}{\partial y} \left(n \cdot \frac{\partial \tilde{C}}{\partial y} \right), \tag{5}$$

\hat{u}, \hat{v} are the fluid velocity components, g represent gravitational acceleration, m deliberate power law index, σ show the electrical conductivity, ν symbolize the kinematic viscosity, ρ_f deliberate the fluid density, ρ_p elaborate the nanoparticles mass density, ρ_m present the density of microorganisms particles, β indicate the thermal expansion volumetric coefficient, D_B , signifies the coefficient of Brownian diffusion, D_T , deliberate the coefficient of thermophoresis diffusion, D_n present the diffusivity of microorganisms, C_p indicate specific heat, k_T present thermal conductivity, τ is the nanoparticles capacities ratio, qr is the radiative heat flux, C present nanoparticle concentration, C_w indicate the concentration at wall, C_∞ symbolize ambient concentration, T, T_w, T_∞ signifies the fluid temperature, wall temperature, and ambient temperature respectively, Wc elaborate the constant speed of cell swimming, n, n_w, n_∞ , represent motile microorganisms density, microorganisms concentration at surface, and ambient motile microorganisms respectively.

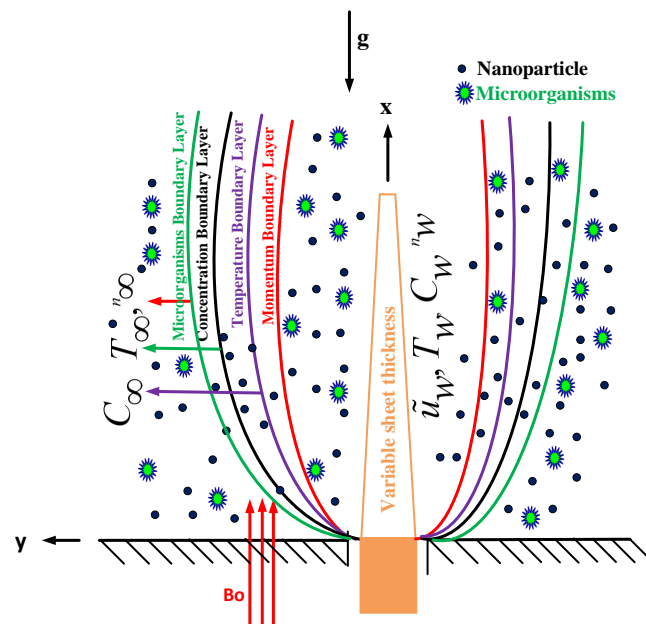


Figure 1. Physical representation of problem.

We get by assuming that the thermophysical variables κ_T have a linear temperature dependence are

$$k_T = k \left(1 + \Lambda_k \left(\frac{T - T_\infty}{T_w - T_\infty} \right) \right), \tag{6}$$

using the Rosseland approximation for radiation [43], the radiative heat flux is simplified as

$$q_r = - \frac{4\sigma_e}{3\beta_R} \frac{\partial T^4}{\partial y}, \tag{7}$$

where, β_R is the coefficient of mean absorption, σ_e is the Stefan-Boltzmann constant. T^4 may be identified by extending in a Taylor series around T_∞ while neglecting higher order expressions given as

$$T^4 \approx 4T_\infty^4 T - 3T_\infty^4. \tag{8}$$

In view of Equations (7) and (8), we obtain

$$\frac{\partial q_r}{\partial y} = \frac{16\sigma_e T_\infty^3}{3\beta_R} \left(\frac{\partial^2 \tilde{T}}{\partial y^2} \right), \tag{9}$$

subject to the boundary conditions

$$\left. \begin{aligned} \hat{u} = U_w = U_0(b+x)^n, \hat{v} = 0, T = T_w, C = C_w, n = n_w, \text{ at } y = \frac{\epsilon(x)}{2}, \\ \lim_{y \rightarrow \infty} \hat{u} = 0, \lim_{y \rightarrow \infty} T = \lim_{y \rightarrow \infty} C = \lim_{y \rightarrow \infty} n = \infty. \end{aligned} \right\} \tag{10}$$

The following similarity transformations [40] are used to simplify the given problem

$$\left. \begin{aligned} \hat{u} &= U_w(x+b)^n F'(\xi), \hat{\vartheta} = \sqrt{-\left(\frac{(n+1)v_\infty U_0(x+b)^{n-1}}{2}\right)} \left(F(\xi) + \frac{n-1}{n+1} \xi F'(\xi)\right), \\ \xi &= \left(\frac{(n+1)U_0(x+b)^{n-1}}{2v_\infty}\right)^{1/2} y, \psi = \left(\frac{2v_\infty U_0(x+b)^{n+1}}{(n+1)}\right) F(\xi), G(\xi) = \frac{T-T_\infty}{T_w-T_\infty}, \\ H(\xi) &= \frac{C-C_\infty}{C_w-C_\infty}, \vartheta(\xi) = \frac{n-n_\infty}{n_w-n_\infty}. \end{aligned} \right\} \quad (11)$$

Equation (1) is satisfied in view of Equation (11), and Equations (2)–(5) become:

$$((1-m) + mWe f'') f''' - \frac{2n}{n+1} F'^2 + FF'' - \frac{2M}{n+1} F' + \omega[G - NrH - Rb\vartheta] = 0 \quad (12)$$

$$(1 + Rd)G'' + PrFG' + \Lambda_k GG'' + \Lambda_k G'^2 + NbG'H' + NtG'^2 = 0, \quad (13)$$

$$H'' + LePrFH' + \frac{Nt}{Nb} G'' = 0, \quad (14)$$

$$\vartheta'' + PrLbF\vartheta' - Pe[\vartheta'H' + \Omega H'' + H''\vartheta] = 0. \quad (15)$$

The associative boundary constraints become

$$\left. \begin{aligned} \lim_{\xi \rightarrow \chi} F(\xi) &= \frac{1-m}{1+m} \chi, \lim_{\xi \rightarrow \chi} F'(\xi) = \lim_{\xi \rightarrow \chi} G(\xi) = \lim_{\xi \rightarrow \chi} H(\xi) = \lim_{\xi \rightarrow \chi} \vartheta(\xi) = 1, \\ \lim_{\xi \rightarrow \infty} F'(\xi) &= \lim_{\xi \rightarrow \infty} G(\xi) = \lim_{\xi \rightarrow \infty} H(\xi) = \lim_{\xi \rightarrow \infty} \vartheta(\xi) = 0. \end{aligned} \right\} \quad (16)$$

Set the following possible change for additional simplifications,

$$\left\{ \begin{aligned} \xi &= \eta + \chi, \\ F(\xi) &= F(\eta + \chi) = f(\eta), \\ G(\xi) &= G(\eta + \chi) = g(\eta), \\ H(\xi) &= H(\eta + \chi) = h(\eta), \\ \vartheta(\xi) &= \vartheta(\eta + \chi) = \zeta(\eta). \end{aligned} \right. \quad (17)$$

As a result, the nonlinear differential Equations (12)–(15) are changed to

$$((1-m) + mWe f'') f''' + f'' f - \frac{2n}{n+1} f'^2 - Mf' + \lambda[g - Nr h - Rb\zeta] = 0, \quad (18)$$

$$(1 + Rd)g'' + Prfg' + \Lambda_k g g'' + \Lambda_k g'^2 + Nbg'h' + Ntg'^2 = 0, \quad (19)$$

$$h'' + LePrfh' + \frac{Nt}{Nb} g'' = 0, \quad (20)$$

$$\zeta'' + PrLbf\zeta' - Pe[\zeta'h' + \Omega h'' + h''\zeta] = 0, \quad (21)$$

along modified boundary constraints:

$$\left. \begin{aligned} \lim_{\eta \rightarrow 0} f(\eta) &= \frac{1-n}{1+n} \chi, \lim_{\eta \rightarrow 0} f_\eta(\eta) = \lim_{\eta \rightarrow 0} g(\eta) = \lim_{\eta \rightarrow 0} h(\eta) = \lim_{\eta \rightarrow 0} \zeta(\eta) = 1, \\ \lim_{\eta \rightarrow \infty} f'(\eta) &= \lim_{\eta \rightarrow \infty} g(\eta) = \lim_{\eta \rightarrow \infty} h(\eta) = \lim_{\eta \rightarrow \infty} \zeta(\eta) = 0, \end{aligned} \right\} \quad (22)$$

where $We = \sqrt{\frac{\Gamma^2(n+1)U_w^3}{\nu}}$ indicate the Weissenberg number, $M = \frac{\sigma B_0^2}{U_0 \rho}$ indicates the magnetic parameter, $Le = \frac{k}{D_B}$ delegate Lewis number, $Rb = \frac{(\rho_m - \rho_f)(n_w - n_\infty)}{\beta \rho (1 - C_\infty)(T_w - T_\infty)}$ represents the bioconvection Rayleigh number, $Nb = \frac{\tau D_B (C_w - C_\infty)}{k}$ indicates the Brownian motion,

$\lambda = \frac{2g\beta(1-C_\infty)(T_w-T_\infty)}{U_w^2(m+1)}$ delegates the mixed convection, $Nr = \frac{(\rho_p-\rho_f)(C_w-C_\infty)}{\beta\rho(1-C_\infty)(T_w-T_\infty)}$ deliberate the buoyancy parameter, $Pr = \frac{(\rho c_p)\nu}{k}$ is the prandtl number, $Nt = \frac{\tau D_T(T_w-T_\infty)}{T_\infty k}$ denotes the thermophoresis parameter, $\chi = c\left(\frac{U_0(m+1)}{2\nu_\infty}\right)^{\frac{1}{2}}$ represent the wall thickness parameter, $Lb = \frac{k}{D_N}$ delegates the Lewis number, $Pe = \frac{dW_c}{D_N}$ indicates the Peclet number, $Rd = \frac{16\sigma_e T_\infty^3}{3\beta_R k}$ elaborates the radiation parameter, $\Omega = \frac{n_\infty}{(n_w-n_\infty)}$ indicates the density ratio of the motile microorganisms.

3. Physical Quantities

The influence of the significant engineering parameters may be adequately investigated in this physical problem by calculating the localized magnitude of drag forces and the rate of thermal transport at the slender sheet. In terms of C_{fx} (skin friction), Nu_x (Nusselt number), Sh_x (Sherwood number), and Nn_x (density of microorganisms) are as follows:

$$C_{fx} = \frac{2\tau_w}{\rho_f U_w^2(x)}, \tag{23}$$

$$Nu_x = \frac{(x+b)q_w}{k(T_w - T_\infty)}, \tag{24}$$

$$Sh_x = \frac{(x+b)q_m}{D_B(C_w - C_\infty)}, \tag{25}$$

$$Nn_x = \frac{(x+b)q_n}{D_n(n_w - n_\infty)}, \tag{26}$$

$\tau_w, q_w, q_m,$ and $q_n,$ respectively,

$$\tau_w = \mu(1-m)\left(\frac{\partial \tilde{u}}{\partial y}\right)_{y=\frac{\epsilon(x)}{2}} + \mu \frac{m\Gamma}{\sqrt{2}} \left(\frac{\partial \tilde{u}}{\partial y}\right)_{y=\frac{\epsilon(x)}{2}}, \tag{27}$$

$$q_w = -\left(k_T + \frac{16\sigma_e T_\infty^3}{3\beta_R}\right) \left(\frac{\partial T}{\partial y}\right)_{y=\frac{\epsilon(x)}{2}}, \tag{28}$$

$$q_m = -D_B \left(\frac{\partial C}{\partial y}\right)_{y=\frac{\epsilon(x)}{2}}, \tag{29}$$

$$q_n = -D_n \left(\frac{\partial n}{\partial y}\right)_{y=\frac{\epsilon(x)}{2}}. \tag{30}$$

The following expressions are derived by utilizing Equations (10), (11) and (17),

$$Re_x^{\frac{1}{2}} C_{fx} = -\left(\sqrt{\frac{n+1}{2}}\right) \left((1-m)f''(0) - \frac{mWe}{2} f''(0)^3 \right), \tag{31}$$

$$Re_x^{-\frac{1}{2}} Nu_x = -\left(\sqrt{\frac{n+1}{2}}\right) (\Lambda_k g(0) + (1+Rd))(g'(0)), \tag{32}$$

$$Re_x^{-\frac{1}{2}} Sh_x = \left(\sqrt{\frac{n+1}{2}}\right) (-h'(0)), \tag{33}$$

$$Re_x^{-\frac{1}{2}} Nn_x = \left(\sqrt{\frac{n+1}{2}}\right) (-\zeta'(0)). \tag{34}$$

4. Solution Procedure

The system of coupled nonlinear differential Equations (8)–(11) along with the boundary conditions (Equation (12)) is solved numerically using the shooting technique together with fourth-order Runge–Kutta integration scheme by converting it into an initial value

problem. The higher order derivatives involved in the finally governing equations are reduced to construct first order differential systems as below: Refs. [44,45]

$$\begin{aligned}
 s_1' &= s_2, \\
 s_2' &= s_3, \\
 s_3' &= \frac{(-1)}{((1-m)+mWe s_3)} [s_1 s_3 - \frac{2n}{n+1} s_2^2 - Ms_2 + \lambda(s_4 - Nrs_6 - Rbs_8)], \\
 s_4' &= s_5, \\
 s_5' &= \frac{(-1)}{(1+Rd)+\Lambda_k s_4} [Prs_1 s_5 + \Lambda_k s_5^2 + Nbs_5 s_7 - Nts_5^2], \\
 s_6' &= s_7, \\
 s_7' &= (-1) [LePrs_1 s_7 + \frac{Nt}{Nb} s_5'], \\
 s_8' &= s_9 \\
 s_9' &= (-1) [LbPrs_1 s_9 - Pe(\Omega s_7' + s_7' s_8 + s_7 s_9)].
 \end{aligned}$$

The corresponding boundary conditions are as follows:

$$\begin{aligned}
 s_1 &= \frac{1-n}{1+n} \chi, \quad s_2 = 1, \quad s_4 = 1, \quad s_7 = 1, \quad s_9 = 1, \quad \text{at } \eta = 0, \\
 s_2 &\rightarrow 0, \quad s_4 \rightarrow 0, \quad s_7 \rightarrow 0, \quad s_9 \rightarrow 0, \quad \text{as } \eta \rightarrow \infty.
 \end{aligned}$$

5. Results and Discussion

The precise analytical formulations of the velocity, energy, concentration, and microorganisms boundary layer are complicated to discover in the ensuing nonlinear differential set of coupled ordinary differential equations. A numerical approach based on the Runge–Kutta method along shooting technique was employed here to yield the solution to this problem. First of all, the validity of the numerical scheme was established in the limiting case to compare with the existing studies on skin friction [40,46] (see Table 1) and Nusselt number [40,47,48] (see Table 2). A close agreement of the two sets (present and previous) of the result provided confidence in the numerical procedure.

Table 1. Comparative of $C_{fx} Re_x^{\frac{1}{2}}$ for various values of m by ignoring other parameters.

n	Fang [46]	Wakif [40]		(Our Results)		
	$\chi = 0.5$	$\chi = 0.25$	$\chi = 0.5$	$\chi = 0.25$	$\chi = 0.5$	$\chi = 0.25$
10	1.1433	1.0603	1.143320620	1.060324666	1.143329	1.060330
9.0	1.1404	1.0589	1.140392519	1.058915794	1.140397	1.058925
7.0	1.1323	1.0550	1.132285178	1.055044823	1.132299	1.055048
5.0	1.1186	1.0486	1.118590381	1.048611306	1.118582	1.048608
3	1.0905	1.0359	1.090492254	1.035868282	1.090510	1.035864
2.0	1.0614	1.0234	1.061402505	1.023407744	1.061410	1.023410

Table 2. Comparing the current numerical findings for Pr when and all others parameter are zero.

Pr	Mabood [47]	Wang [48]	Wakif [40]	(Our Results)
0.70	0.4539	0.4539	0.45391	0.4544
2.00	0.9114	0.9114	0.91135	0.9113
7.00	1.8954	1.8954	1.89540	1.8954
20	3.3539	3.3539	3.35390	3.3539
70	6.4622	6.4622	6.46219	6.4621

Table 3 deliberated for skin friction coefficient $-f''(0)$, it is observed that local index number m , Weissenberg number We , magnetic parameter M , Nr and Rb erected the skin friction and it reduced when mixed convection λ enhanced, and opposite behavior can be observed for Nusselt number $-g'(0)$ in Table 4. While thermophoretic parameter Nt diminished for $-\theta'(0)$. Sherwood’s number improved for Le and Nb , while lowered for Nt

represented in Table 5. The density of motile microorganisms enhanced for bioconvection parameter Pe, Lb, Ω (see Table 6).

Table 3. Numerical outcomes for $Re_x^{\frac{1}{2}} C_{fx} = -\left(\sqrt{\frac{n+1}{2}}\right)\left((1-m)f''(0) - \frac{mWe}{2}f''(0)^3\right)$.

m	We	M	λ	Nr	Rb	$-f''(0)$
0.1	0.3	1.0	0.3	0.3	1.8	1.3351
0.2						1.3593
0.3						1.4441
	0.3					1.3351
	0.4					1.3579
	0.5					1.3815
		1.0				1.3351
		2.0				1.4904
		3.0				1.6352
			0.1			1.4080
			0.2			1.3709
			0.3			1.3351
				0.3		1.3351
				0.4		1.3391
				0.5		1.3431
					1.6	1.3274
					1.7	1.3312
					1.8	1.3351

Table 4. Numerical outcomes for $Re_x^{\frac{-1}{2}} Nu_x = -\left(\sqrt{\frac{n+1}{2}}\right)(\Lambda_k g(0) + (1 + Rd))(g'(0))$.

m	We	M	λ	Nr	Rb	Nb	Nt	Λ_k	Rd	$-g'(0)$
0.1	0.3	1.0	0.3	0.3	1.8	0.1	0.1	0.3	0.1	0.6895
0.2										0.6726
0.3										0.6506
	0.3									0.6895
	0.4									0.6888
	0.5									0.6880
		1.0								0.6895
		2.0								0.6634
		3.0								0.6400
			0.1							0.6768
			0.2							0.6835
			0.3							0.6895
				0.3						0.6895
				0.4						0.6889
				0.5						0.6882
					1.6					0.6908
					1.7					0.6902
					1.8					0.6895
						0.1				0.6895
						0.2				0.5690
						0.3				0.4659
							0.1			0.6895
							0.2			0.6928
							0.3			0.6956
								0.1		0.6895
								0.2		0.5986

Table 4. Cont.

<i>m</i>	<i>We</i>	<i>M</i>	λ	<i>Nr</i>	<i>Rb</i>	<i>Nb</i>	<i>Nt</i>	Λ_k	<i>Rd</i>	$-g'(0)$
								0.3		0.5302
									0.1	0.9229
									0.2	0.7902
									0.3	0.6895

Table 5. Numerical outcomes for $Re_x^{-\frac{1}{2}} Nn_x = \left(\sqrt{\frac{n+1}{2}}\right)(-h'(0))$.

<i>Le</i>	<i>Nt</i>	<i>Nb</i>	$-\phi'(0)$
1.0	0.1	0.1	1.1542
2.0			1.8501
3.0			2.3063
	0.1		1.1542
	0.2		0.8741
	0.3		0.5779
		0.1	1.1542
		0.2	1.3317
		0.3	1.3859

Table 6. Numerical outcomes for $Re_x^{-\frac{1}{2}} Nn_x = \left(\sqrt{\frac{n+1}{2}}\right)(-\zeta'(0))$.

<i>Pe</i>	<i>Lb</i>	Ω	$-\chi'(0)$
0.1	0.3	0.1	0.7897
0.2			0.8911
0.3			0.9937
	0.1		0.3855
	0.2		0.6133
	0.3		0.7897
		0.1	0.7897
		0.2	0.7983
		0.3	0.8069

The decelerated flow in the face of improving the strength of magnetic field *M* is caused due to the Lorentz force shown in Figure 2a. This reactive force comes to play its role when the magnetic field interacts with an electric field. This decreasing flow helps the conservation of loss of kinetic energy to heat energy and, hence, the improvement in temperature is shown in Figure 2b. Figure 3a delineates the impact of power-law index *m* on $f'(\eta)$ (velocity distribution). The velocity of higher inputs of *m* is lowered for rising inputs of *m*, while energy is upsurged. Physically it is due to the stretched surface being heated. As a result, the fluid loses additional heat, and the fluid temperature $g(\eta)$ rises depicted in Figure 3b. Figure 4a show the impact of the Weissenberg number *We* on momentum $f'(\eta)$. For maximum inputs of the *We*, the momentum boundary layer of tangent hyperbolic nanofluid is lowered. The temperature boundary layer of the nanofluid is valued for gradually increasing Weissenberg number *We* values. Physically, it is the ratio between relaxation time and processing time. Improving the *We* means it enhances the relaxation time, which causes improvement of $g(\eta)$ portrayed in Figure 4b.

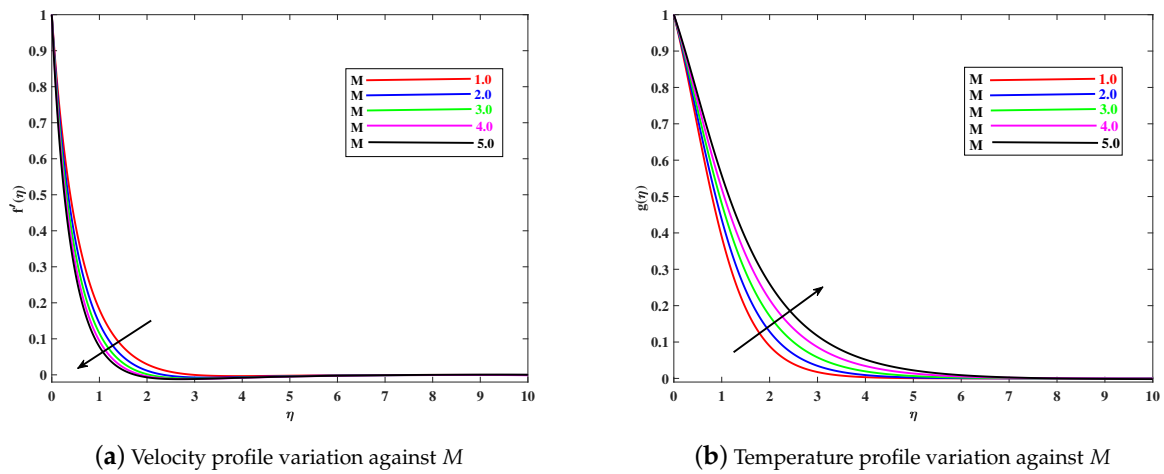


Figure 2. Effect of M to influence the momentum and thermal profile.

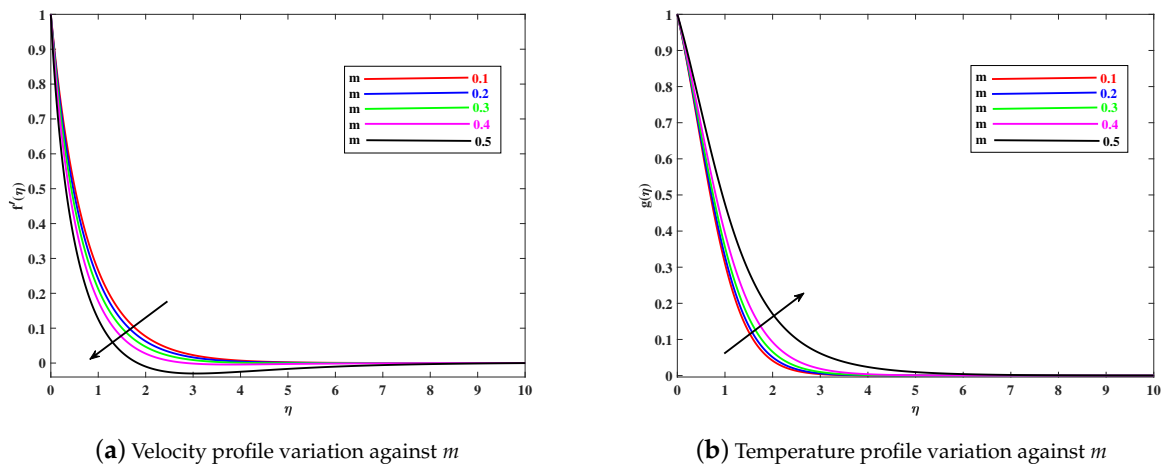


Figure 3. Effect of m to influence the momentum and thermal profile.

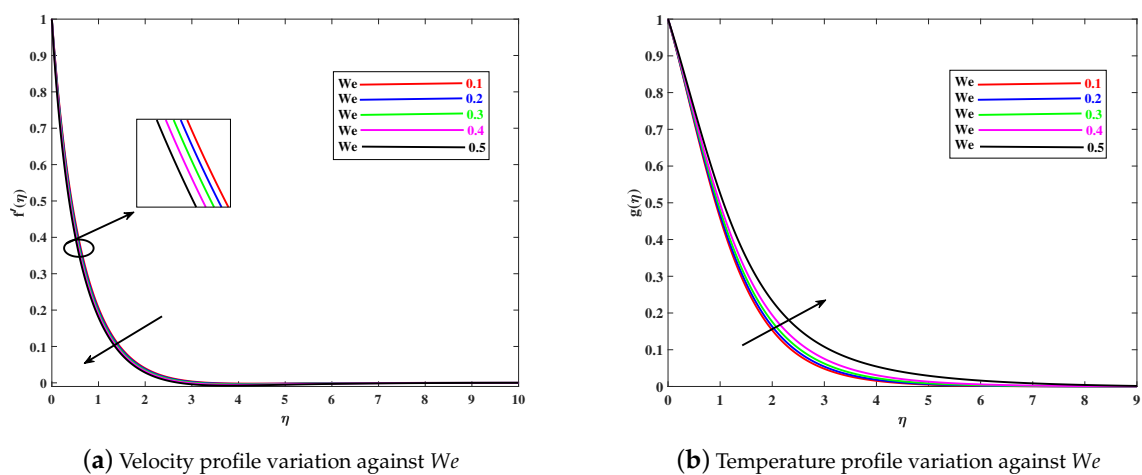


Figure 4. Effect of We to influence the momentum and thermal profile.

The role of mixed convection parameter λ on velocity is depicted in Figure 5a. It is observed that enhanced in λ intensified the momentum curve $f'(\eta)$ and lessened the temperature profile $g(\eta)$ portraits in Figure 5b. Physically, an increase in λ strong the buoyancy influence. The effect of bioconvection Rayleigh number Rb on momentum is portrayed in Figure 6a. The increment in Rb lowered the velocity curve $f'(\eta)$ and promoted

the energy curve $g(\eta)$. Because it is reciprocal to $(T_w - T_\infty)$. Thus, the buoyancy impacts reduced the boundary flow and raised the temperature delineated in Figure 6b. The impact of Nb on the energy boundary layer is delineated in Figure 7a. The higher inputs of Nb on energy curve $g(\eta)$ boosted and hindered the concentration boundary layer $h(\eta)$ portraits in Figure 7b. Physically, the faster motion of nanoparticles gained the heat conduction.

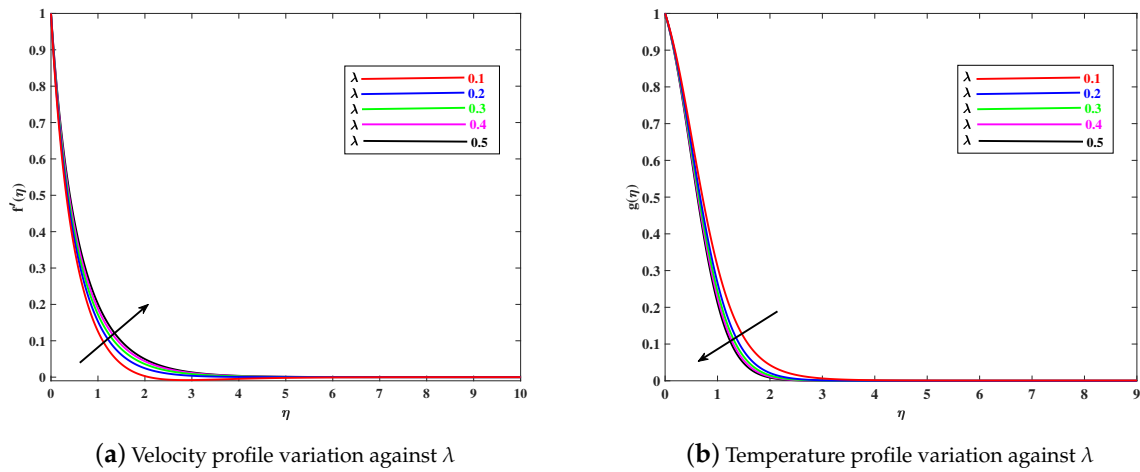


Figure 5. Effect of λ to influence the momentum and thermal profile.

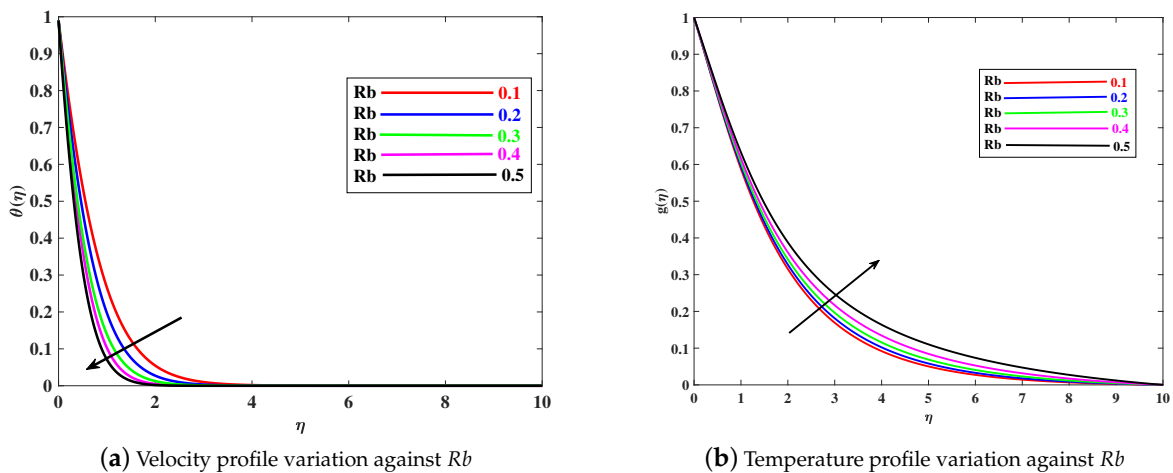


Figure 6. Effect of Rb to influence the momentum and thermal profile.

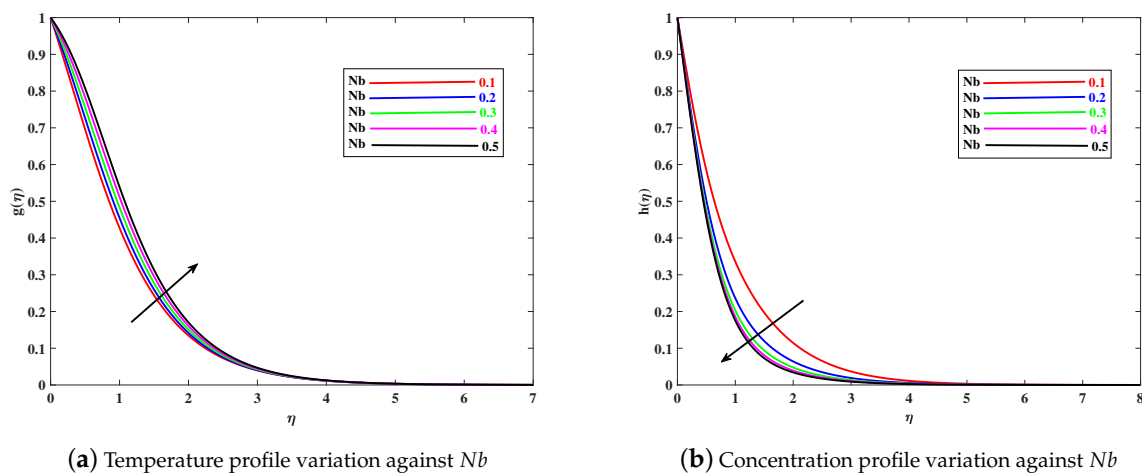


Figure 7. Effect of Nb to influence the thermal and concentration profile.

The role of the Thermophoretic parameter Nt on the temperature of nanoparticles is deliberated in Figure 8a. The higher inputs of Nt improved the thermal distribution $g(\eta)$ and concentration distribution $h(\eta)$ delineated in Figure 8b. Physically, the thermophoresis effect refers to the movement of nanoparticles from a higher to a lower temperature, consequently increasing temperature and concentration. The impact of radiation Rd on thermal distribution $g(\eta)$. It is observed that higher values of Rd improved the thermal boundary layer. Physically, it is due to higher inputs of Rd mean larger heat diffusion, which causes the thermal boundary layer can be seen in Figure 9a. The larger inputs of Lb can be seen. It is observed that lowered the microorganism boundary layer $\zeta(\eta)$ is portrayed in Figure 9b. The influence of Peclet number Pe on microorganisms boundary layer $\zeta(\eta)$ is depicted in Figure 10a. The bioconvection flow is diminished with the higher Peclet number. This occurs physically because the advection transport rate is greater than the diffusive transport rate. The influence of microorganisms density ratio Ω on bioconvection boundary layer $\zeta(\eta)$ can be portrayed in Figure 10b. The higher values of Ω reduced the bioconvection curve $\zeta(\eta)$.

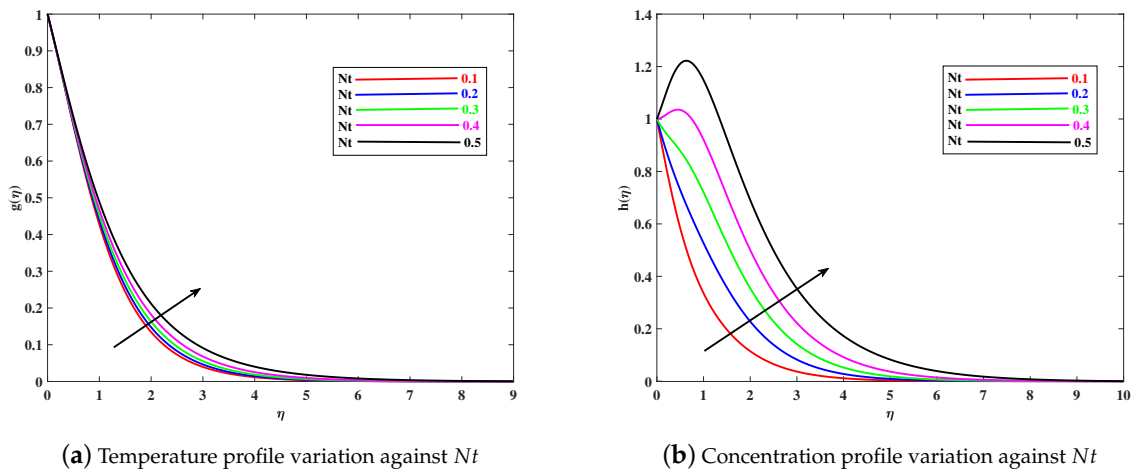


Figure 8. Effect of Nt to influence the thermal and concentration profile.

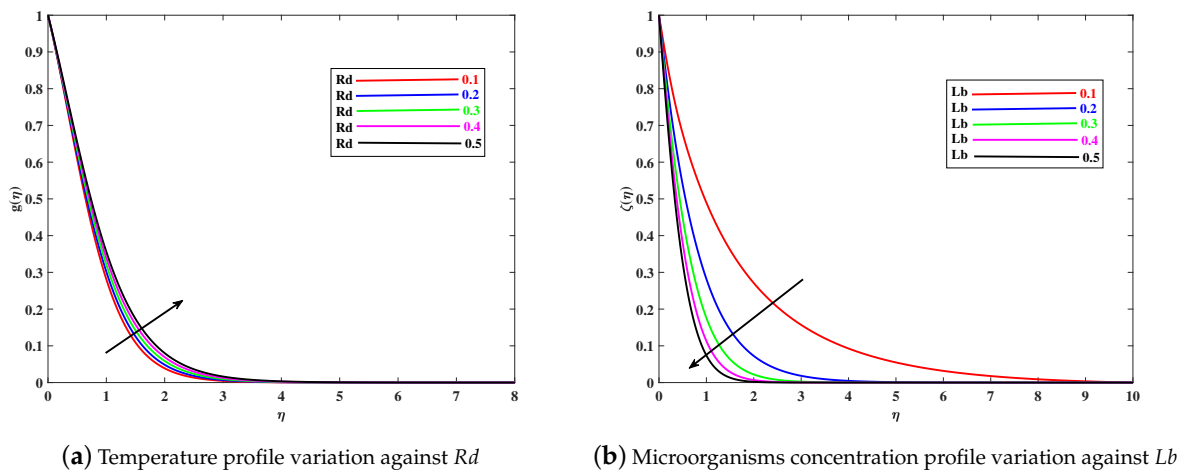
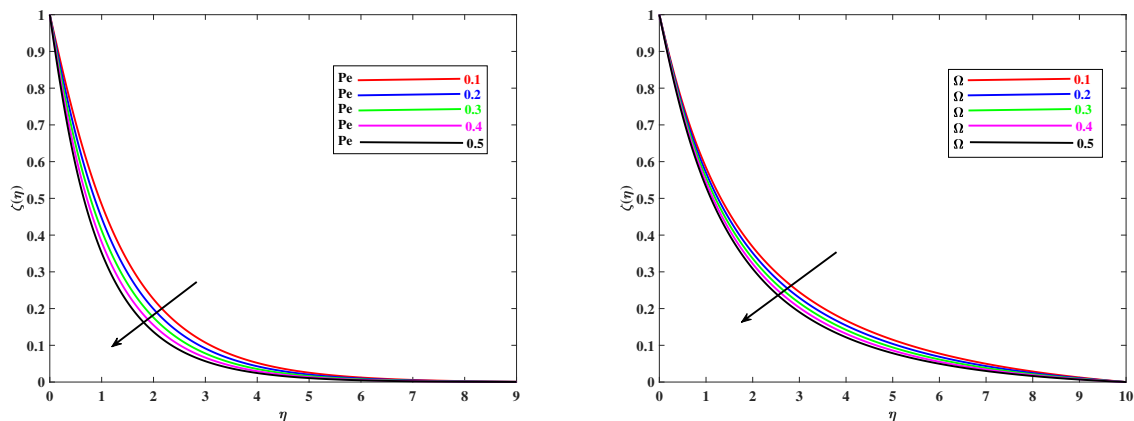


Figure 9. Effect of Rd and Lb to influence the concentration and bioconvection profile.



(a) Microorganisms concentration profile variation against Pe (b) Microorganisms concentration profile variation against Ω

Figure 10. Effect of Pe and Ω to influence the biconvection profile.

6. Conclusions

The numerical investigation of tangent hyperbolic nanofluid flow across a slender elastic sheet of irregular thickness under the impact of a magnetic field is discussed in this study. The Buongiorno model of nanofluids is investigated using the temperature and concentration constitutive equations. The thermophoresis and Brownian motion effects are accounted for in the tangent hyperbolic nanofluid model. The flow phenomena also have gyrotactic bioconvection characteristics. The results are obtained using the Runge-Kutta method approach in the MATLAB platform, and the present results are compared with the past literature to validate the results. The following are the major implications of this problem:

- The fluid velocity $f'(\eta)$ enhance with larger values of the mixed convection (λ), and it reduced with enhance in magnetic number M , Weissenberg number We , bioconvection Rayleigh number Rb , power law index m , because these parameters are responsible to decelerate the flow.
- The temperature profile enhance with Nb (Brownian motion), Rd (Radiation parameter) and Nt (thermophoretic parameter).
- The growing value of thermophoresis responsible to enhance the nanoparticles concentration, but opposite trend is reported against growing value of Brownian motion (Nb).
- The microorganism density is depreciated when the parameters bioconvection Lewis number (Lb), Peclet number (Pe), and density ratio (Ω) are given higher inputs.
- The Skin friction is improved with improving magnetic (M), power index (m), Weissenberg number (We), bioconvection Rayleigh number (Rb), and buoyancy ratio (Nr), and it is decreased with mixed convection (λ) due to the accelerated flow.
- Nusselt number is reduced with higher inputs of power index (m), magnetic (M), Weissenberg number (We), bioconvection Rayleigh number (Rb), Brownian motion (Nb), thermophoresis (Nt), thermal buoyancy (λ), and radiation (Rd), as these parameters enhanced the temperature distribution to reduced Nusselt number.
- Sherwood number is increase with increasing Le , and Nb , but reverse behaviour can be observed in thermophoresis parameter Nt .
- Bioconvection profile for the density of motile microorganisms Ω Peclet number Pe and bioconvection Lewis number Lb diminished for enhanced concentration difference parameter.
- The present results are compared with the past literature to validate the results.

Author Contributions: Author Contributions: M.Z.A. modeled the problem and wrote the manuscript. S.U.R. and S.F. thoroughly checked the mathematical modeling, English corrections, formal analysis, and revision. A.K.H. complete the formal analysis and revision. B.A. solved the problem using MATLAB software. N.A.S. and W.W.: writing—review and editing. All authors finalized the manuscript after its internal evaluation. All authors have read and agreed to the published version of the manuscript.

Funding: This research received no external funding.

Institutional Review Board Statement: Not applicable.

Informed Consent Statement: Not applicable.

Data Availability Statement: Not applicable.

Conflicts of Interest: The authors declare no conflict of interest.

References

1. Awan, A.U.; Ahammad, N.A.; Majeed, S.; Gamaoun, F.; Ali, B. Significance of hybrid nanoparticles, lorentz and coriolis forces on the dynamics of water based flow. *Int. Commun. Heat Mass Transf.* **2022**, *135*, 106084. [[CrossRef](#)]
2. Younis, O.; Alizadeh, M.; Kadhim Hussein, A.; Ali, B.; Biswal, U. Hasani Malekshah, E. MHD natural convection and radiation over a flame in a partially heated semicircular cavity filled with a nanofluid. *Mathematics* **2022**, *10*, 1347. [[CrossRef](#)]
3. Choi, S.U.; Eastman, J.A. *Enhancing Thermal Conductivity of Fluids with Nanoparticles*; Tech. Rep.; Argonne National Lab.: Lemont, IL, USA, 1995.
4. Waqas, H.; Wakif, A.; Al-Mdallal, Q.; Zaydan, M.; Farooq, U.; Hussain, M. Significance of magnetic field and activation energy on the features of stratified mixed radiative-convective couple-stress nanofluid flows with motile microorganisms. *Alex. Eng. J.* **2022**, *61*, 1425–1436. [[CrossRef](#)]
5. Aly, A.M.; Mohamed, E.M.; Alsedais, N. The magnetic field on a nanofluid flow within a finned cavity containing solid particles. *Case Stud. Therm. Eng.* **2021**, *25*, 100945. [[CrossRef](#)]
6. Habib, D.; Salamat, N.; Abdal, S.H.S.; Ali, B. Numerical investigation for mhd prandtl nanofluid transportation due to a moving wedge: Keller box approach. *Int. Commun. Heat Mass Transf.* **2022**, *135*, 106141. [[CrossRef](#)]
7. Jamshed, W. Numerical investigation of MHD impact on Maxwell nanofluid. *Int. Commun. Heat Mass Transf.* **2021**, *120*, 104973. [[CrossRef](#)]
8. Awais, M.; Ullah, N.; Ahmad, J.; Sikandar, F.; Ehsan, M.M.; Salehin, S.; Bhuiyan, A.A. Heat transfer and pressure drop performance of nanofluid: A state-of-the-art review. *Int. J. Thermofluids* **2021**, *9*, 100065. [[CrossRef](#)]
9. Shang, Y.; Dehkordi, R.B.; Chupradit, S.; Toghraie, D.; Sevbitov, A.; Hekmatifar, M.; Suksatan, W.; Sabetvand, R. The computational study of microchannel thickness effects on H₂O/CuO nanofluid flow with molecular dynamics simulations. *J. Mol. Liq.* **2022**, *345*, 118240. [[CrossRef](#)]
10. Dawar, A.; Wakif, A.; Thumma, T.; Shah, N.A. Towards a new mhd non-homogeneous convective nanofluid flow model for simulating a rotating inclined thin layer of sodium alginate-based iron oxide exposed to incident solar energy. *Int. Commun. Heat Mass Transf.* **2022**, *130*, 105800. [[CrossRef](#)]
11. Sabu, A.; Wakif, A.; Areekara, S.; Mathew, A.; Shah, N.A. Significance of nanoparticles' shape and thermo-hydrodynamic slip constraints on mhd alumina-water nanofluid flows over a rotating heated disk: The passive control approach. *Int. Commun. Heat Mass Transf.* **2021**, *129*, 105711. [[CrossRef](#)]
12. Imran, M.; Kamran, T.; Khan, S.A.; Muhammad, T.; Waqas, H. Physical attributes of bio-convection in nanofluid flow through a paraboloid of revolution on horizontal surface with motile microorganisms. *Int. Commun. Heat Mass Transf.* **2022**, *133*, 105947. [[CrossRef](#)]
13. Waqas, H.; Kafait, A.; Muhammad, T.; Farooq, U. Numerical study for bio-convection flow of tangent hyperbolic nanofluid over a riga plate with activation energy. *Alex. Eng. J.* **2022**, *61*, 1803–1814. [[CrossRef](#)]
14. Zhang, X.; Yang, D.; Rehman, M.I.U.; Mousa, A.; Hamid, A. Numerical simulation of bioconvection radiative flow of Williamson nanofluid past a vertical stretching cylinder with activation energy and swimming microorganisms. *Case Stud. Therm. Eng.* **2022**, *33*, 101977. [[CrossRef](#)]
15. Asjad, M.I.; Zahid, M.; Inc, M.; Baleanu, D.; Almohsen, B. Impact of activation energy and MHD on Williamson fluid flow in the presence of bioconvection. *Alex. Eng. J.* **2022**, *61*, 8715–8727. [[CrossRef](#)]
16. Narsimulu, G.; Gopal, D.; Udaikumar, R. Numerical approach for enhanced mass transfer of bio-convection on magneto-hydrodynamic Carreau fluid flow through a nonlinear stretching surface. *Mater. Today Proc.* **2022**, *49*, 2267–2275. [[CrossRef](#)]
17. Habib, D.; Salamat, N.; Abdal, S.; Siddique, I.; Salimi, M.; Ahmadian, A. On time dependent MHD nanofluid dynamics due to enlarging sheet with bioconvection and two thermal boundary conditions. *Microfluid. Nanofluid.* **2022**, *26*, 1–15. [[CrossRef](#)]
18. Shah, S.A.A.; Ahammad, N.A.; Din, E.; E.M.T.; Gamaoun, F.; Awan, A.U.; Ali, B. Bio-convection effects on prandtl hybrid nanofluid flow with chemical reaction and motile microorganism over a stretching sheet. *Nanomaterials* **2022**, *12*, 2174. [[CrossRef](#)] [[PubMed](#)]

19. Habib, D.; Salamat, N.; Ahsan, M.; Abdal, S.; Siddique, I.; Ali, B. Significance of bioconvection and mass transpiration for mhd micropolar maxwell nanofluid flow over an extending sheet. *Waves Random Complex Media* **2022**, 1–15. [[CrossRef](#)]
20. Ali, B.; Ali, M.; Hussain, S.; Yahya, A.U.; Hussain, I. Tangent hyperbolic nanofluid: Significance of lorentz and buoyancy forces on dynamics of bioconvection flow of rotating sphere via finite element simulation. *Chin. J. Phys.* **2022**, *77*, 658–671. [[CrossRef](#)]
21. Ali, L.; Ali, B.; Liu, X.; Ahmed, S.; Shah, M.A. Analysis of bio-convective mhd blasius and sakiadis flow with cattaneo-christov heat flux model and chemical reaction. *Chin. J. Phys.* **2022**, *77*, 1963–1975. [[CrossRef](#)]
22. Hassan, M.; Ali, S.; Aich, W.; Khliissa, F.; Ayadi, B.; Kolsi, L. Transport pattern of non-Newtonian mass and thermal energy under two diverse flow conditions by using modified models for thermodynamics properties. *Case Stud. Therm. Eng.* **2022**, *29*, 101714. [[CrossRef](#)]
23. Selimefendigil, F.; Öztıp, H.F.; Kolsi, L.; Omri, M. Performance analysis of thermoelectric generator mounted chaotic channel by using non-Newtonian nanofluid and modeling with efficient computational methods. *Alexandria Eng. J.* **2022**, *61*, 3527–3549. [[CrossRef](#)]
24. Li, X.; Abidi, A.; Zhao, X.; Gao, X.; Sajadi, S.M.; Sharifpur, M. Investigation of mixed convection of non-Newtonian fluid in the cooling process of lithium-ion battery with different outlet position. *J. Energy Storage* **2022**, *46*, 103621. [[CrossRef](#)]
25. Khader, M.M.; Babatin, M.M.; Megahed, A.M. Numerical study of thermal radiation phenomenon and its influence on amelioration of the heat transfer mechanism through MHD non-Newtonian Casson model. *Coatings* **2022**, *12*, 208. [[CrossRef](#)]
26. Pandey, S.; Yoon, S.Y.; Balachandar, S.; Ha, M.Y. Experimental and numerical investigations of thermal and flow characteristics of a shear-thinning non-Newtonian fluid in a differentially heated cavity. *Int. Heat Mass Transf.* **2022**, *187*, 122570. [[CrossRef](#)]
27. Boukrouche, M.; Debliche, H.; Paoli, L. Unsteady non-Newtonian fluid flows with boundary conditions of friction type: The case of shear thickening fluids. *Nonlinear Anal.* **2022**, *216*, 112701. [[CrossRef](#)]
28. Çolak, A.B. Analysis of the effect of arrhenius activation energy and temperature dependent viscosity on non-Newtonian Maxwell nanofluid bio-convective flow with partial slip by artificial intelligence approach. *Chem. Thermodyn. Therm. Anal.* **2022**, *6*, 100039. [[CrossRef](#)]
29. Khashi'ie, N.S.; Waini, I.; Kasim, A.R.M.; Zainal, N.A.; Ishak, A.; Pop, I. Magnetohydrodynamic and viscous dissipation effects on radiative heat transfer of non-Newtonian fluid flow past a non-linearly shrinking sheet: Reiner–philippoff model. *Alex. Eng. J.* **2022**, *61*, 7605–7617. [[CrossRef](#)]
30. Bhatti, M.; Arain, M.; Zeeshan, A.; Ellahi, R.; Doranehgard, M. Swimming of gyrotactic microorganism in MHD Williamson nanofluid flow between rotating circular plates embedded in porous medium: Application of thermal energy storage. *J. Energy Storage* **2022**, *45*, 103511. [[CrossRef](#)]
31. Al-Farhany, K.; Abdulkadhim, A.; Hamzah, H.K.; Ali, F.H.; Chamkha, A. Mhd effects on natural convection in a u-shaped enclosure filled with nanofluid-saturated porous media with two baffles. *Prog. Nucl. Energy* **2022**, *145*, 104136. [[CrossRef](#)]
32. Bejawada, S.G.; Reddy, Y.D.; Jamshed, W.; Nisar, K.S.; Alharbi, A.N.; Chouikh, R. Radiation effect on MHD Casson fluid flow over an inclined non-linear surface with chemical reaction in a Forchheimer porous medium. *Alex. Eng. J.* **2022**, *61*, 8207–8220. [[CrossRef](#)]
33. Hossain, R.; Azad, A.; Hasan, M.J.; Rahman, M. Thermophysical properties of Kerosene oil-based CNT nanofluid on unsteady mixed convection with MHD and radiative heat flux. *Eng. Sci. Technol. Int. J.* **2022**, *35*, 101095. [[CrossRef](#)]
34. Vishalakshi, A.; Mahabaleshwar, U.; Sheikhnejad, Y. Impact of MHD and mass transpiration on Rivlin–Ericksen liquid flow over a stretching sheet in a porous media with thermal communication. *Transp. Porous Media* **2022**, *142*, 353–381. [[CrossRef](#)]
35. Nazeer, M.; Hussain, F.; Khan, M.I.; El-Zahar, E.R.; Chu, Y.-M.; Malik, M. Theoretical study of MHD electro-osmotically flow of third-grade fluid in micro channel. *Appl. Math. Comput.* **2022**, *420*, 126868. [[CrossRef](#)]
36. Venkata Ramana, K.; Gangadhar, K.; Kannan, T.; Chamkha, A.J. Cattaneo–Christov heat flux theory on transverse MHD Oldroyd-B liquid over nonlinear stretched flow. *J. Therm. Anal. Calorim.* **2022**, *147*, 2749–2759. [[CrossRef](#)]
37. Famakinwa, O.; Koriko, O.; Adegbe, K.; Omowaye, A. Effects of viscous variation, thermal radiation, and arrhenius reaction: The case of MHD nanofluid flow containing gyrotactic microorganisms over a convectively heated surface. *Partial. Differ. Equations Appl. Math.* **2022**, *5*, 100232. [[CrossRef](#)]
38. Fetecau, C.; Shah, N.A.; Vieru, D. General solutions for hydromagnetic free convection flow over an infinite plate with newtonian heating, mass diffusion and chemical reaction. *Commun. Theor. Phys.* **2017**, *68*, 768. [[CrossRef](#)]
39. Hillesdon, A.; Pedley, T. Bioconvection in suspensions of oxytactic bacteria: Linear theory. *J. Fluid Mech.* **1996**, *324*, 223–259. [[CrossRef](#)]
40. Wakif, A. A novel numerical procedure for simulating steady MHD convective flows of radiative Casson fluids over a horizontal stretching sheet with irregular geometry under the combined influence of temperature-dependent viscosity and thermal conductivity. *Math. Probl. Eng.* **2020**, *2020*, 1675350. [[CrossRef](#)]
41. Ferdows, M.; Zaimi, K.; Rashad, A.M.; Nabwey, H.A. Mhd bioconvection flow and heat transfer of nanofluid through an exponentially stretchable sheet. *Symmetry* **2020**, *12*, 692. [[CrossRef](#)]
42. Khan, M.; Hussain, A.; Malik, M.; Salahuddin, T.; Khan, F. Boundary layer flow of MHD tangent hyperbolic nanofluid over a stretching sheet: A numerical investigation. *Results Phys.* **2017**, *7*, 2837–2844. [[CrossRef](#)]
43. Rosseland, S. *Astrophysik: Auf Atomtheoretischer Grundlage*; Springer: Berlin/Heidelberg, Germany, 2013; Volume 11.

44. Rehman, S.U.; Mariam, A.; Ullah, A.; Asjad, M.I.; Bajuri, M.Y.; Pansera, B.A.; Ahmadian, A. Numerical computation of buoyancy and radiation effects on mhd micropolar nanofluid flow over a stretching/shrinking sheet with heat source. *Case Stud. Therm. Eng.* **2021**, *25*, 100867. [[CrossRef](#)]
45. Wang, F.; Asjad, M.I.; Ur Rehman, S.; Ali, B.; Hussain, S.; Gia, T.N.; Muhammad, T. MHD Williamson nanofluid flow over a slender elastic sheet of irregular thickness in the presence of bioconvection. *Nanomaterials* **2021**, *11*, 2297. [[CrossRef](#)] [[PubMed](#)]
46. Fang, T.; Zhang, J.; Zhong, Y. Boundary layer flow over a stretching sheet with variable thickness. *Appl. Math. Comput.* **2012**, *218*, 7241–7252. [[CrossRef](#)]
47. Mabood, F.; Khan, W.; Ismail, A.M. MHD boundary layer flow and heat transfer of nanofluids over a nonlinear stretching sheet: A numerical study. *J. Magn. Magn. Mater.* **2015**, *374*, 569–576. [[CrossRef](#)]
48. Wang, C. Free convection on a vertical stretching surface. *ZAMM-J. Appl. Math. Mech. Angew. Math. Mech.* **1989**, *69*, 418–420. [[CrossRef](#)]